NUCLEIC ACID THERAPEUTICS
Volume 00, Number 00, 2023

DOI: 10.1089/nat.2023.0015

Delivery Characterization of SPL84 Inhaled Antisense Oligonucleotide Drug for 3849 + 10 kb C- > T Cystic Fibrosis Patients

Efrat Ozeri-Galai, PhD,[1,*] Lital Friedman, MSc,[1,*] Ofra Barchad-Avitzur, PhD,[1] Matthew R. Markovetz, PhD,[2] William Boone, PhD,[2] Kaitlyn R. Rouillard, PhD,[2] Chava D. Stampfer, MSc,[1] Yifat S. Oren, PhD,[1] David B. Hill, PhD,[2,3] Batsheva Kerem, PhD,[1,4] and Gili Hart, PhD[1]

Recent advances in the therapeutic potential of RNA-related treatments, specifically for antisense oligonucleotide (ASO)-based drugs, have led to increased numbers of ASO regulatory approvals. In this study, we focus on SPL84, an inhaled ASO-based drug, developed for the treatment of the pulmonary disease cystic fibrosis (CF). Pulmonary drug delivery is challenging, due to a variety of biological, physical, chemical, and structural barriers, especially when targeting the cell nucleus. The distribution of SPL84 throughout the lungs, penetration into the epithelial cells and nucleus, and structural stability are critical parameters that will impact drug efficacy in a clinical setting. In this study, we demonstrate broad distribution, as well as cell and nucleus penetration of SPL84 in mouse and monkey lungs. *In vivo* and *in vitro* studies confirmed the stability of our inhaled drug in CF patient-derived mucus and in lung lysosomal extracts. The mobility of SPL84 through hyperconcentrated mucus was also demonstrated. Our results, supported by a promising preclinical pharmacological effect of full restoration of cystic fibrosis transmembrane conductance regulator channel activity, emphasize the high potential of SPL84 as an effective drug for the treatment of CF patients. In addition, successfully tackling the lung distribution of SPL84 offers immense opportunities for further development of SpliSense's inhaled ASO-based drugs for unmet needs in pulmonary diseases.

Keywords: distribution, antisense oligonucleotide, mucus, cystic fibrosis

Introduction

Antisense oligonucleotides (ASOs) are single-strand, small synthetic nucleic acid molecules that can bind to specific sequences within target RNA molecules. ASOs are usually 16–25 bases long and are designed to hybridize with RNA through Watson–Crick base pairing. ASOs can have different modes of action, one of which is splice switching. Splice switching ASOs consist of chemically modified nucleotides, which ablate RNase H activity and allow interaction with nuclear pre-mRNA during the splicing process [1].

These ASOs can be designed to bind to 5′ or 3′ splice junctions or to splicing enhancer or silencer sites, blocking the RNA–RNA base pairing or protein–RNA binding interactions that occur between components of the splicing machinery and the pre-mRNA [2,3]. The benefit of ASO-mediated therapies is targeting the disease source at the RNA level offering a promising alternative to therapies targeting downstream processes. Advances made in the development of splice switching ASO-based drugs led to the marketing approval of five splice switching ASO-based drugs for two rare diseases, Duchenne muscular dystrophy and spinal muscular atrophy, in the recent years [4–6].

SPL84 is an inhaled ASO drug with the 2′-O-methoxyethyl (2′-O-MOE) phosphorothioate chemical modification, developed for the treatment of cystic fibrosis (CF) patients carrying the 3849 + 10 kb C- > T (3849) *cystic fibrosis transmembrane conductance regulator (CFTR)* mutation. The 3849 mutation

[1]SpliSense, Biohouse Labs, Haddasah Ein Kerem, Jerusalem, Israel.
[2]Marsico Lung Institute and [3]Joint Department of Biomedical Engineering, UNC Chapel Hill, Chapel Hill, North Carolina, USA.
[4]Department of Genetics, The Hebrew University, Jerusalem, Israel.
*These authors contributed equally to this work.

is a splicing mutation leading to the inclusion of a cryptic exon harboring a premature termination codon (PTC) in the mRNA. The PTC leads to degradation of a significant fraction of the mRNA by the nonsense-mediated mRNA decay mechanism, as well as to the production of truncated nonfunctional CFTR proteins. The 3849 is the seventh and eighth most common CFTR mutation in the United States and Europe, respectively, with >1500 patients in the United States and Europe combined carrying at least one 3849 allele [7,8].

Currently, there are no approved drugs that specifically target the 3849 mutation. There are two Food and Drug Administration (FDA)-approved CFTR modulator drugs available for CF patients carrying the 3849 mutation—Kalydeco® and Symdeko®—and one approved CFTR modulator drug for CF patients compound heterozygous for the 3849 mutation and another qualifying mutation—Trikafta® [9–11]. However, these drugs have limited efficacy on lung function in 3849 CF patients [10,12,13].

A battery of *in vitro* studies showed that the treatment with SPL84 modulates splicing of the *CFTR pre-mRNA* resulting in an increase of correctly spliced *CFTR RNA* and full-length CFTR proteins. Moreover, pharmacological studies with SPL84 demonstrated its efficiency and potency, as reflected by full restoration of CFTR function in human nasal epithelial and human bronchial epithelial (HBE) cells derived from CF patients carrying the 3849 mutation, measured using the Ussing chamber assay [14]. This assay serves as the gold standard for efficacy assessment of CF drugs, due to the limitations and lack of CF animal models [15,16], and is considered as a strong predictor of patient response to CF treatments [15,17,18].

The key challenge for ASO-based therapeutics is the delivery of the ASO to its target tissue and to specific cells, while minimizing exposure of other tissues. As SPL84 is delivered to the lung via inhalation, bridging between the promising *in vitro* data of SPL84 in patient-derived airway cells and *in vivo* lung delivery and distribution was a key in moving SPL84 into the clinic (Phase 1 study successfully completed, Phase 2 study to be initiated shortly). The lung architecture is commonly visualized as a bunch of grapes formed by 23 serial bifurcations from the trachea to the last alveolar duct, with 85%–90% occupied by alveoli [19]. The translocation of oligonucleotide-based drugs across the pulmonary mucosal epithelia is hampered by several biological barriers including the mucus layer, tight epithelial cell junctions, and mucociliary clearance mechanisms designed to remove inhaled particulates from the airway [20].

In the present study, SPL84 is shown to be stable in CF sputum and lung lysosomal extracts. Wide distribution of SPL84 is demonstrated in mouse and monkey lungs following inhalation. Furthermore, SPL84 is shown to penetrate pathological mucus, enter various respiratory epithelial cell types, and reach the targeted cell nucleus in both *in vitro* and *in vivo* models.

Materials and Methods

Synthesis of ASO

SPL84 is a uniformly modified 2-O-(2-methoxyethyl) phosphorothioate ASO composed of 19 nucleotide bases, in the form of a sodium salt. SPL84 was manufactured at BioSpring (Frankfurt, Germany). For the monkey study, SPL84 was manufactured at LGC Biosearch Technologies Inc. [Petaluma, CA, USA (FDA EI 3011897291)]. SPL84 was dissolved in 0.9% sodium chloride (pH 7.4; Baxter)/phosphate-buffered saline (PBS) at the desired concentration for *in vitro* or *in vivo* studies. SPL84 sequence is as follows: CUGCAACAGAUGGAAGACU.

Migration of SPL84 in mucus

HBE mucus was prepared from pooled washings from >50 cell cultures from >10 normal, nonsmoking donors in accordance with UNC Chapel Hill Institutional Review Board protocols. The washings were concentrated in dialysis tubing against Spectra gel to reach 8% (w/v) solids, as previously described [21]. Mucus was diluted to 2% and 4% solids. The diffusion of Cy5-labeled SPL84 through buffer (PBS) or mucus was quantified using the 1-directional migration assay, as previously described [22]. Mucus at 2, 4, or 8% solids (40 μL) was loaded into a 0.7-mm inner diameter glass capillary tube (VitroCom), injected with 1 μL of matched concentration of mucus with Cy5-labeled SPL84 (1 mg/mL), and sealed with a 1:1:1 mixture of Vaseline, lanolin, and paraffin (Valap).

Tubes were placed into a custom-built, three-dimensional-printed 384-well plate maintained at 37°C, and fluorescence was measured with a Tecan fluorometer. Well intensity was measured every 15 min for 24–48 h. Controls were prepared by measuring the diffusion of 5 kDa fluorescein isothiocyanate (FITC)-dextran in buffer and at each mucus concentration. In addition, the diffusion of Cy5-labeled SPL84 in buffer (PBS) was measured. Similarly, the diffusive motion of lipid nanoparticles (LNP; CDL6002F-DD from CD Bioparticles, New York) [23] was measured to show the effect of size on diffusive motion. For each condition, $n \geq 3$ capillary tubes were separately prepared and evaluated.

Data Analysis. The diffusion coefficient, and thereby effective viscosity of the ASO in mucus, was determined by fitting the intensity pattern for each capillary tube to a Gaussian function of the form:

$$I = I_0 e^{-(x-x_0)^2/2Dt} \quad (1)$$

where I is the measured intensity of the ASO as a function of distance along the capillary tube, I_0 is the intensity at the center of the Gaussian, x is the measured distance down the capillary tube, x_0 is the position of the center of the Gaussian, D is the diffusion coefficient of the ASO in mucus, and t is the time at which the measurement is taken. From the diffusion coefficient, the effective viscosity (η) of the probe particle was calculated by the Stokes Einstein relationship:

$$\eta = 2k_B T/6\pi r D \quad (2)$$

where k_B is the Boltzmann constant, T is the absolute temperature in Kelvin, and r is the radius of the probe particle.

The penetration time through mucus was calculated by a simplified version of the Stokes Einstein relationship between the mean squared displacement:

$$MSD = 2Dt;\ t = MSD/2D \quad (3)$$

Applying this equation, it is predicted that a particle with a diffusion coefficient of 50 $\mu m^2/s$ would be able to penetrate a 100-μm-thick mucus layer in 200 s.

Statistical analysis. Statistical analysis of the effective viscosity of SPL48 was performed using Student's *t*-test. Results from SPL84 were compared with the effective viscosity of the molecule in PBS as well as with the effective viscosity of FITC-labeled dextran. A pairwise Pearson's test was used to determine if the viscosity of SPL84 and FITC-labeled dextran is correlated with concentration.

Stability of SPL84 in rat lung lysosomal lysate and northern blot analysis

SPL84 working solution was mixed on ice with rat lung lysosomal lysate (RLuLL) (XENOTECH) in the presence of protease inhibitor cocktail (Calbiochem Set III). Protease inhibitor was added to protect nucleases from degradation. The resulting solution was incubated at 37°C, and aliquots were drawn at 5 and 30 min, 3, 8 and 24 h, transferred to a fresh tube, and immediately frozen in liquid nitrogen (the final concentration of SPL84 in the collection tubes is 5 μM). As a control to evaluate RLuLL nuclease potency, a nuclease nonresistance double-strand RNA molecule was treated under the same conditions. Evaluation of SPL84 structural stability was performed by northern blot analysis. The SPL84 samples from each of the four incubation time points were diluted with loading sample buffer, boiled for 5 min at 95°C, and removed immediately to ice.

Each sample was run on denaturing gels. Equivalent amounts of SPL84 from working solution were similarly treated and loaded on each gel as a positive control for gel migration of a non-degraded ASO. Blotted membranes were hybridized with 3′-labeled digoxigenin locked nucleic acid (LNA) probe (the sequence: AG + TCT + TCCA + TCTG + TTGCAG-Dig, ''+'' = LNA modification) and detected with anti-DIG-HRP-Ab (anti-digoxigenin-POD Fab fragment; Roche). Membranes were exposed to an X-ray film and developed. Comparisons to the untreated control SPL84 were performed to evaluate the structural stability as a function of exposure time in RLuLL. This analysis was performed at Quark Pharmaceutical (Ness Ziona, Israel).

Stability of SPL84 in CF sputum

Sputum from 10 (5 female, 5 male) individuals with CF acquired from the UNC Adult Pulmonary Clinic (Chapel Hill, NC, USA) was pooled, mixed by trituration, and then rotated for 24 h at 4°C [21]. SPL84 was spiked into the pooled human sputum at final concentrations of 5 μM and incubated (triplicates) for 1, 3, 6, 8, 24, and 48 h at 37°C in the presence of protease inhibitor cocktail (Calbiochem Set III). Protease inhibitor was added to protect nucleases from degradation.

At the specified time points, 50 μL aliquots were transferred to nuclease-free Eppendorf tubes and immediately frozen at −80°C until analysis. Evaluation of SPL84 stability was performed by northern blot analysis with the same 3′-labeled digoxigenin LNA probe, as described previously. This analysis was performed at Quark Pharmaceuticals (Ness Ziona).

Amplification, differentiation, migration, and pharmacological activity of SPL84 in HBE primary cells

HBE cells (from non-CF or CF donors) were expanded by growing the cells in PneumaCult™-Ex Plus Medium (AMP medium). After expansion, cells were seeded on porous filters (6.5 mm Transwell® with 0.4-μm Pore Polyester Membrane Insert 0.33 cm^2 Transwell; Corning) in air–liquid interface (ALI) culture. After cell differentiation under ALI conditions, SPL84 was added from the apical side (on top of the mucus).

Localization and accumulation of SPL84 in cell nuclei. Forty-eight hours from the last ASO addition, the filters of non-CF HBE cells were fixed for analysis of localization and accumulation of SPL84. Vectashield mounting medium containing 4′,6-diamidino-2-phenylindole (DAPI) was added, and the filter was placed on a microscope slide. Slices were imaged using an FV-1200 confocal microscope (Olympus, Japan). For image analysis, the ImageJ software was used.

Migration of SPL84 through mucus to HBE cells. Fluorescent time-lapse imaging of SPL84 kinetics following apical treatment of live non-CF HBE cells. The cells were not washed for a week, allowing the accumulation of a mucus layer, after which 35 μM Cy5-SPL84 was added on top of the mucus. Time-lapse fluorescent images of Cy5-SPL84 were captured immediately after the addition of Cy5-SPL84. Cells were stained with calcein. Images were taken using the FV-1200 confocal microscope (Olympus).

Electrophysiological experiments—Ussing chamber assay. The short-circuit current (Isc) was measured under voltage clamp conditions with an EVC4000 precision V/I Clamp (World Precision Instruments). Culture inserts with differentiated HBE cells were mounted in Ussing chambers (Physiologic Instruments). For all measurements, chloride (Cl^-) concentration gradient across the epithelium was applied by differential composition of basal and apical physiological solutions.

Inhibitors and activators were added after stabilization of baseline Isc: sodium (Na^+) channel blocker amiloride (100 μM; Sigma–Aldrich) to inhibit apical epithelial Na+ channel (ENaC); cAMP agonists forskolin (10 μM; Sigma–Aldrich) and IBMX (100 μM; Sigma–Aldrich) to activate the transepithelial cAMP-dependent current (including Cl^- transport through CFTR channels); CFTR inhibitor CFTRinh172 (10 μM; Sigma–Aldrich) to specifically inhibit CFTR; and ATP (100 μM; Sigma–Aldrich) to challenge the purinergic calcium-dependent Cl^- secretion. CFTR-specific activity was quantified according to the effect of CFTR inhibitor Inh-172, which enables determining the relative current contribution of the CFTR channels versus other anion transport pathways [24].

RNA purification. Total RNA from HBE cells was extracted using the QIAshredder and RNeasy micro-Kit (Qiagen). Complementary DNA (cDNA) synthesis was performed using the High-Capacity cDNA Kit (Applied Biosystems). For the evaluation of the cryptic exon skipping, we employed reverse transcription-polymerase chain reaction (PCR) to amplify the correctly and aberrantly spliced transcripts using primers aligned to exons 22 and 23, using Platinum™ SuperFi™ Green PCR Master Mix (Invitrogen). PCR primers are as follows: F-5′-ATAGCTTGATGCGATCTGTGA-3′ (exon 22) and R-5′-ATCCAGTTCTTCCCAAGAGGC-3′ (exon 23).

Animal experiments

Animal management. Mice experiments were performed at a Contract Research Organization specializing in preclinical research and services, Science in Action (Weizmann Science Park, Ness Ziona). Animal handling was performed according to the guidelines of the National Institutes of Health (NIH) and the Association for Assessment and Accreditation of Laboratory Animal Care (AAALAC). CD-1 mice (Envigo) at a standard age (~6–8 weeks) at the outset of the study were used for the wild-type (WT) mice experiments. These experiments included only female mice, which is beneficial for mice handling during anesthesia and intratracheal (IT) procedures. For the β-ENaC experiments, C57BL/6N littermates of β-ENaC mice O'Neal colony CB6088 (WT mice) and C57BL/6N Scnn1b-Tg O'Neal colony CB6088 (β-ENaC mice) were used [25] (Marsico Lung Institute, UNC Chapel Hill, NC, USA).

The monkey experiments were performed at ITR Laboratories (Quebec, Canada). All animal procedures were conducted according to the Animal Care Committee (ACC) of ITR. All animals used in the study were cared for in accordance with the principles outlined in the current ''Guide to the Care and Use of Experimental Animals'' as published by the Canadian Council on Animal Care and the ''Guide for the Care and Use of Laboratory Animals,'' an NIH publication. Male young adult cynomolgus monkeys (*Macaca fascicularis*) (Worldwide Primates Inc.) were used in the experiment.

IT administration of SPL84 in mice. For IT administrations of SPL84, the CD-1 mice were anesthetized and hung vertically by a rubber band, which holds the upper incisors. The mouse tongue was gently pulled out using forceps and a volume of 30/50 μL of SPL84 or vehicle control was delivered directly into the trachea, and the mouse was allowed to recover immediately. SPL84 was dissolved and diluted in sterile saline/PBS under sterilized conditions.

The doses in the WT mice experiments were 0.2, 1, 2, 5, and 10 mg/kg. SPL84 was administrated once or thrice (every other day) as indicated.

The experimental group sizes were as follows: For the distribution experiments—saline ($n=2$), 0.2 mg/kg SPL84 ($n=3$), 1 mg/kg SPL84 ($n=3$), 2 mg/kg SPL84 ($n=3$). For the kinetics studies over 1 and 4 weeks—all group sizes were identical, $n=2$. For the β-ENaC experiments—all group sizes of C57BL/6N β-ENaC and C57BL/6N Scnn1b-Tg mice in the two doses were identical, $n=3$, except the saline group, $n=1$.

Sample collection and tissue processing for histopathology. The mice were sacrificed with carbon dioxide at the time specified for each group. The lungs with trachea were processed to slides for histopathologic evaluation; the lungs were filled slowly with formalin, and the lungs and trachea were then removed into a test tube with 10% neutral-buffered formalin. For the WT CD-1 mice, necroscopy and lung sampling were performed 48 h after the final dose. For the kinetics studies, the lungs were collected 1, 3, 5, 7, 14, or 28 days after the final dose. For the β-ENaC experiments, the lungs were collected from WT and β-ENaC mice 24 h after the final dose.

Inhalation administration to the cynomolgus monkey. The inhalation route of administration was chosen because it is the route of administration of the test item in human clinical studies. SPL84 was administered via inhalation by oronasal face mask exposure. Monkeys were dosed once a week for 4 weeks, at achieved dose levels of 1.8 and 24.6 mg/kg/week (two males/dose). The achieved dose was determined by analysis of aerosol filter samples using a validated analytical method. Three sections [hilum of the lung (entrance of the main bronchus), middle part of the lung (including secondary bronchi), and most peripheral part of the lung] from each side of the lung were collected at necropsy (Fig. 5A), 72 h after the final dose, fixed in neutral-buffered 10% formalin for 48 h, and then embedded in paraffin wax for *in situ* hybridization (ISH) analysis.

ISH analysis

Five-micrometer sections were prepared and mounted onto glass slides. SPL84 was detected on sections by hybridizing to a digoxigenin (DIG)-labeled 2′-O-methyl (2′-OMe) RNA probe detected with alkaline phosphatase-labeled anti-Dig polyclonal Ab (Roche Diagnostics). After hybridization, sections were lightly counterstained with Nuclear Fast Red, as described previously [26]. This analysis was performed at Smart Assays Biotechnologies Ltd. (Ness Ziona).

Semiquantitative analysis of the extent of the hybridization signal throughout the respiratory epithelium was performed; the approximate percentage of the labeled epithelium surface was established, and hybridized sections were blindly evaluated and graded according to the following scale:

- Grade 0: 0%–10%
- Grade 1: 10%–25%
- Grade 2: 25%–50%
- Grade 3: 50%–75%
- Grade 4: 75%–90%
- Grade 5: 90%–100%

Results

SPL84 rapidly migrates through the mucus barrier under healthy, moderate, and severe disease conditions and is not degraded in CF sputum

Since CF is characterized by the accumulation of a thick mucus layer covering the airways, as a first step in evaluating the SPL84 delivery efficiency, the stability and mobility of SPL84 in mucus were evaluated in a set of *in vitro* analyses. First, the migration of fluorescently labeled SPL84 in mucus harvested from HBE cell cultures was analyzed. The mucus was prepared to reach concentrations that mimic healthy (2% solids), mild CF (4% solids), and severe CF (8% solids) conditions. Due to the polymeric nature of mucus, all measurements of the mucus physical properties are dependent on the length scale of the tested particles (Fig. 1A). The effective viscosity (η) is the resistance to motion the particle experiences and is inversely correlated with its ability to migrate through mucus.

Thus, the viscosity that is calculated for the particle in mucus will have a higher value if the particle is larger than the mesh size (i.e., size exclusion barrier) or if it interacts with the mucus (e.g., electrostatic interactions). The data presented in Fig. 1B indicate that the effective viscosity for Cy5-labeled SPL84 increased with mucus concentration,

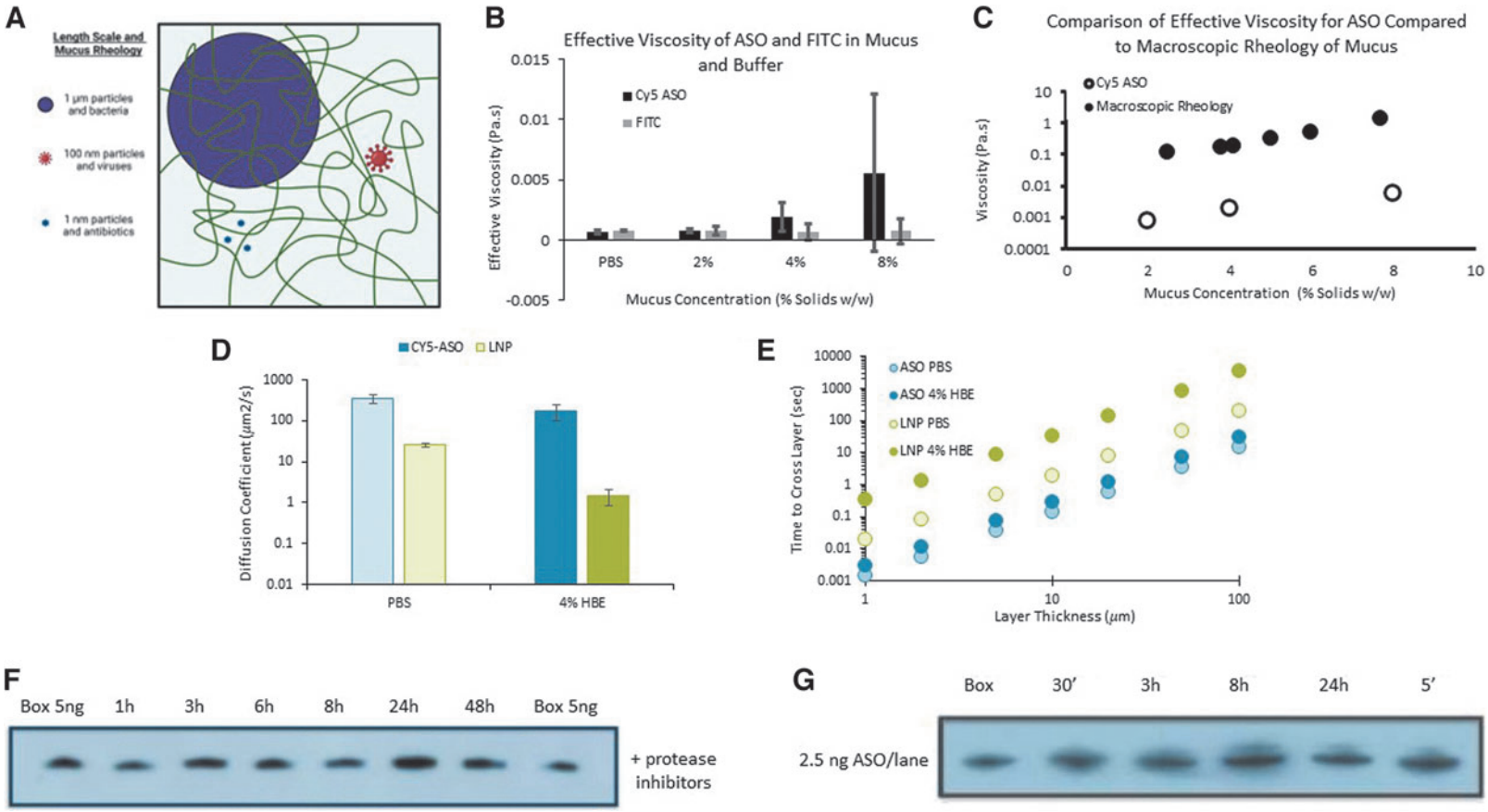

FIG. 1. SPL84 demonstrates structural stability, mobility, and penetration in CF sputum. **(A)** Characteristic length scales of mucus. The polymeric mucin glycoproteins within mucus create a mesh-like gel. If the probe particle is larger than the mesh size of mucus (*purple*, 1-µm bacterial-like probe), the results will be similar in magnitude to macroscopic results. If the probes are near the mesh size of mucus (*red*, 100-nm virus and LNP-like probes) they will report the microscopic properties of both the mucus gel and fluid. If the probes are much smaller than the mesh size, like the small molecules (*purple*, ~1 nm antibiotic/drug delivery), the probes will measure the rheological properties of the fluid component of mucus, not the polymeric properties. Figure created with Biorender.com. **(B)** Effective viscosity of ASO and FITC in mucus and buffer. The diffusion coefficient of Cy5-SPL48 (*black*); the microscopic properties of both the mucus gel and fluid are reported. If the probes are much smaller than the mesh size, like the small molecules (*blue*, ~1 nm antibiotic/drug delivery), the probes will measure the rheological properties of the fluid component of mucus, not the polymeric properties, and FITC (*gray*) was measured and converted into the effective viscosity of each molecule in buffer (PBS), 2, 4, and 8% mucus via the Stokes Einstein relationship [Eq. (2)]. **(C)** Comparison of the effective viscosity for SPL84 (*white circle*, Cy5 ASO) compared with macroscopic rheology of mucus, as measured in a previous study (*full black circle*) [27]. **(D)** Diffusion coefficients calculated from the intensity pattern of Cy5-labeled ASO (*blue*) and commercially available LNPs (*green*). Data indicate that the smaller size of ASOs relative to LNPs results in a drastical increase of these particles ability to diffuse in both buffer and mucus. **(E)** Time to cross a mucus layer as a function of layer thickness. The smaller size of ASOs allows them to permeate through a mucus layer much faster than LNPs can penetrate PBS. **(F)** Autoradiograms of northern blots following incubation of SPL84 (5 µM) in mucus from CF patients at different time points; all samples were exposed to protease inhibitors. Box = positive control (SPL84 spiked in mucus from CF patients at 4°C was used for size control). **(G)** Northern blot of SPL84 samples incubated in RLuLL for up to 24 h. All samples were exposed to protease inhibitors Box = positive control; untreated SPL84. ' = minutes; ASO, antisense oligonucleotide; CF, cystic fibrosis; FITC, fluorescein isothiocyanate; LNPs, lipid nanoparticles; PBS, phosphate-buffered saline; RLuLL, rat lung lysosomal lysate.

indicating a potential interaction with mucus. This increase in nanoscopic viscosity was ~100-fold lower than macroscopic mucus viscosity, or the viscosity of mucus that is associated with the gel-forming mucins (Fig. 1C). These nanoscopic data are in agreement with previously published fluorescence recovery after photobleaching studies, which determined that 70 kDa FITC-dextran only interacted with the low viscosity fluid within the mucus mesh and did not experience the bulk viscosity of mucus [21,27].

By measuring the diffusion of SPL84 in PBS, it was determined that the SPL84 radius is ~1 nm, which is in agreement with the diffusion of the 5 kDa FITC-dextran reported previously [22]. Furthermore, these data confirmed that while SPL84 interacts with the mucus mesh, these interactions are weak in nature and will not affect its penetration of even a pathological mucus layer. Based on the measured diffusion coefficients, the maximum penetration time predicted in 8% mucus (mimicking severe CF) is 85 s (Supplementary Table S1).

Other emerging RNA/DNA-based therapies for CF, involving longer, larger, and more complex oligonucleotides or RNA molecules, require delivery systems to penetrate to the lung epithelial cells. One common vehicle for the delivery of mRNA replacement therapies is based on encapsulated LNPs. To compare the permeation of SPL84 with LNPs, we tested the migration of commercially available LNPs and SPL84 in buffer and in 4% HBE mucus. Measurements in buffer demonstrate that, primarily due to the small size of SPL84, we see a nearly two-log fold increase in the diffusion coefficient of SPL84 relative to LNPs (Fig. 1D), indicating that SPL84 diffuses more effectively than the LNPs.

This trend holds even when both are tested in 4% mucus. The time for each molecule to traverse a mucus layer has a strong dependence on the size of the molecule. This suggests that SPL84 will be able to penetrate through a CF-like mucus layer more readily than the LNPs will migrate in buffer (Fig. 1E). When evaluated in 8% mucus, the LNPs had no measurable migration even after 72 h, in contrary to SPL84 (Supplementary Table S1), indicating that the size exclusion barrier of severe CF-like mucus sufficiently trapped and inhibited the motion of the LNPs (data not shown). Together these data confirm the potential superiority of ASO lung delivery over standard size LNPs and motivate the use of ASOs for inhaled delivery in pathological mucus as they penetrate and are delivered more efficiently than LNPs.

Following the migration analysis, the structural stability of SPL84 was further evaluated in the presence of sputum samples taken from CF patients. As shown in Fig. 1F, the structural integrity of SPL84 was maintained when spiked into CF sputum for up to 48 h, as indicated from the single band in an equivalent position to that of the positive control sample. These results are aligned with the high stability of 2′-O-MOE-modified ASOs [28].

Stability of SPL84 in rat lung lysosomal lysate

ASOs have been shown to enter cells through high- and low-binding plasma protein receptors on the cell surface, resulting in ASO compartmentalization into lysosomes and endosomes, as part of the natural process of endocytosis [29]. A lysosome can break down many kinds of biomolecules via its hydrolytic enzymes and its specific composition of both membrane proteins and lumenal proteins, combined with extreme acidic conditions (lumen pH of ~4.5–5.0). Therefore, we assessed the structural stability of SPL84 when spiked into RLuLL. Results showed that SPL84 incubated in RLuLL appears to be nuclease resistant and pH resistant for at least 24 h, as indicated by the migration of the single oligonucleotide band to a position equivalent to that of the positive control sample (Fig. 1G). In contrast, when a control nuclease non-resistant dsRNA was incubated in RLuLL, smaller migration bands, indicating degradation, appeared within 3 h of incubation (Supplementary Fig. S1). These results indicate that SPL84 is stable in lysosomal lysate and suggests protection from degradation under acidic conditions or in the presence of nucleases.

SPL84 rapidly penetrates and migrates through healthy and CF mucus to the epithelial cell nuclei, leading to restoration of CFTR function

We additionally assessed the penetration of naked SPL84 through mucus generated in HBE cells from both non-CF and CF patients (carrying the 3849 mutation), grown in a two-dimensional structure in ALI culture. Upon cell differentiation, a pseudostratified epithelial layer is formed, consisting of a mixture of ciliated and mucus-secreting epithelial cells, leading to the secretion of a mucus layer at the apical side of the cells. Fluorescently labeled SPL84 was administered on top of the mucus layer at the apical side of the non-CF HBE cells. SPL84 showed efficient penetration through the mucus layer into the HBE cells (Fig. 2A). Importantly, SPL84 could be detected in the cell nuclei, where splicing modulation of the pre-mRNA takes place (Fig. 2B), confirming target engagement.

Following the demonstration of successful penetration through the mucus layer and uptake by the epithelial cells and nuclei, we assessed SPL84 activity as reflected by modulation of *CFTR pre-mRNA* and channel function in HBE cells from a patient homozygous for the 3849 mutation. As shown in Fig. 2C, SPL84 treatment from the apical side of the HBE cells, which is more relevant in a clinical setting of an inhaled drug and addresses the issue of mucus layer penetration, properly modulates the *CFTR pre-mRNA*, leading to the generation of full-length WT *CFTR RNA* and to impressive restoration of CFTR activity, as measured by the Ussing assay.

The cumulative *in vitro* studies demonstrate the structural and functional stability of SPL84 in CF sputum as well as the efficient mobility in mucus and uptake of the naked SPL84 by the epithelial cell nuclei. Following the *in vitro* analyses, further *in vivo* studies were performed to evaluate the distribution, migration, and penetration of SPL84 in the target organ, the lungs.

Broad pulmonary distribution and epithelial cell nuclei penetration of SPL84 in the WT mouse lungs

To evaluate the delivery of SPL84 to the lungs *in vivo*, SPL84 distribution was first analyzed in WT mice. To this end, mouse lung sections were analyzed by ISH labeling following intratracheal administration at three doses: 0.2, 1, and 2 mg/kg. At all tested doses, a high proportion of respiratory epithelial cells accumulated a detectable amount of SPL84 throughout the entire lung, with a dose-related increase in the staining intensity (Fig. 3A). Higher magnitude

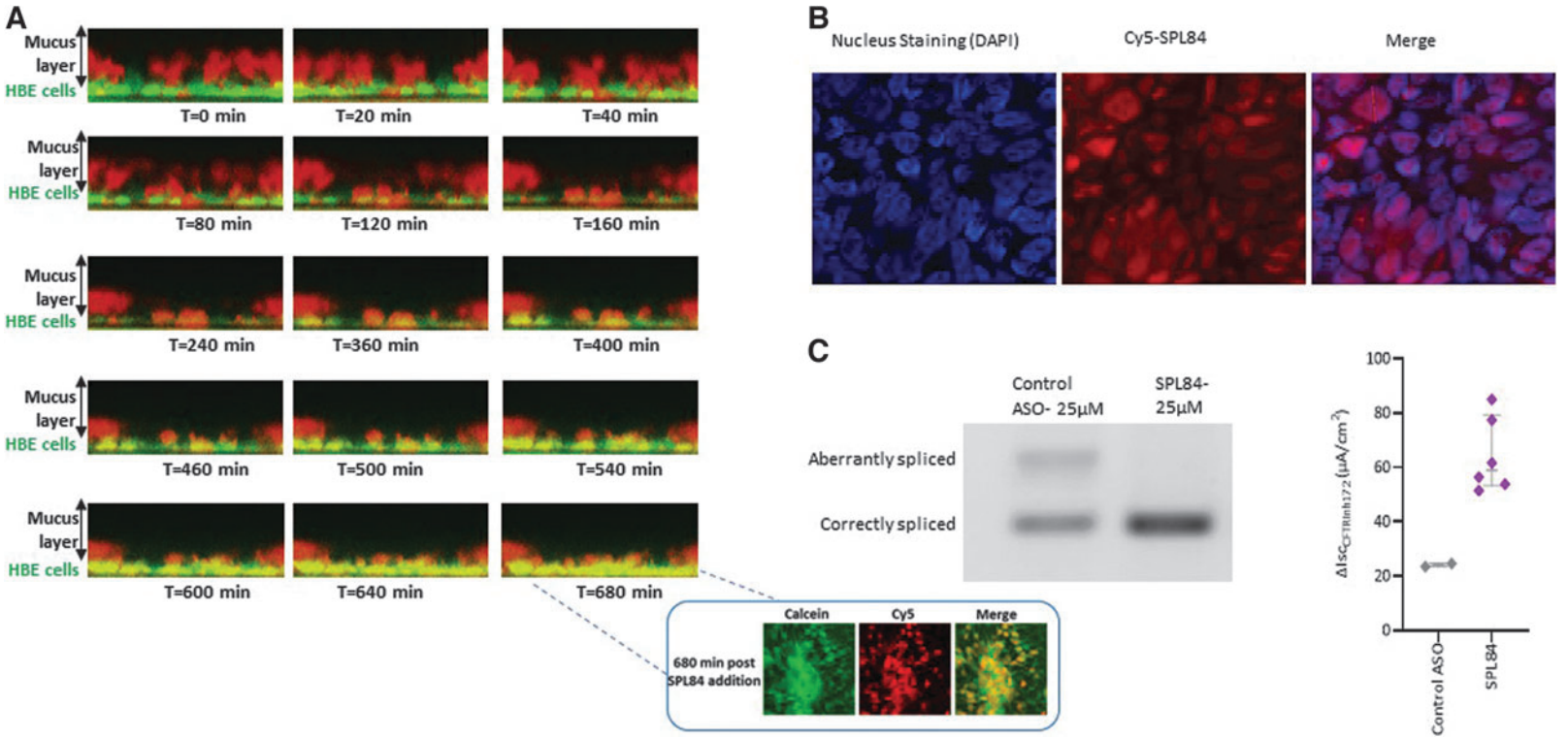

FIG. 2. Rapid penetration of SPL84 through healthy and CF mucus, and localization in the cell nuclei leads to the generation of full-length WT CFTR RNA and restoration of CFTR activity. HBE cells grown in a 2D structure in ALI culture were differentiated by PneumaCult Growth Protocol. **(A)** Time-lapse fluorescence images of the migration of Cy5-SPL84 through mucus into non-CF HBE cells following differentiation during apical treatment on top of the mucus. Fluorescent images of Cy5-SPL84 are presented every 20 min following the addition of 35 μM Cy5-SPL84. Cy5-SPL84 is shown in *red*, HBE cells (calcein) are shown in *green*, and overlay of Cy5-SPL84 and HBE cells is shown in *yellow*. Single optical section from $T = 680$ min is presented in a *blue square*. **(B)** Non-CF HBE cells were differentiated, followed by apical treatment on top of the mucus with three additions of 50 μM Cy5-SPL84. Forty-eight hours after the last addition, the cells were fixed and visualized for detection of SPL84. The fluorescent signal was detected using a Cy5 filter under confocal microscope. Nuclei were stained with DAPI. **(C)** The effect on the CFTR splicing pattern was analyzed using RT-PCR showing the aberrantly and correctly spliced CFTR transcripts following apical treatment of 25 μM SPL84 in HBE cells derived from 3849 homozygous patient (*left panel*). Scatter dot plot of absolute values of ΔISCCFTRinh172 (μA/cm^2) using Ussing chamber assay (*right panel*). The *gray thick horizontal line* marks the median. 2D, two-dimensional; ALI, air–liquid interface; CFTR, cystic fibrosis transmembrane conductance regulator; DAPI, 4′,6-diamidino-2-phenylindole; HBE, human bronchial epithelial; RT-PCR, reverse transcription-polymerase chain reaction; WT, wild type.

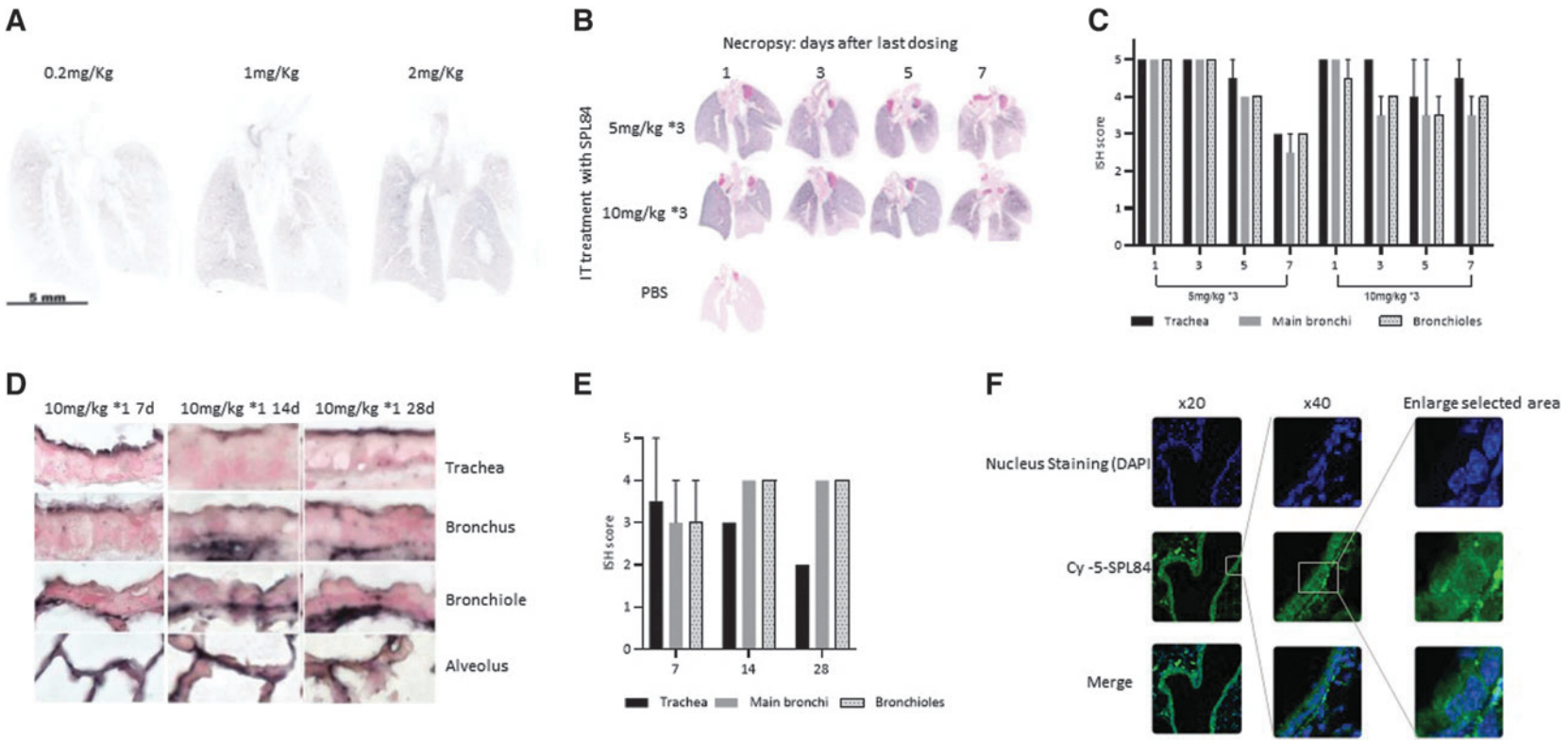

FIG. 3. Broad pulmonary delivery and distribution kinetics of SPL84 in WT mouse lungs. **(A)** SPL84 localization detected by ISH analysis. Low-power scans of fixed mouse lung sections following IT administration at three different doses; representative lung sections from all experimental groups are shown. **(B)** Low-power scans of lung sections from kinetics study over 1 week, treated as indicated with three IT administrations of 5 or 10 mg/kg of SPL84. **(C)** Semiquantitative analysis of the extent of hybridization signal throughout the respiratory epithelium (described in detail in the Materials and Methods ''ISH analysis'' section). **(D)** High-power microphotographs of representative lung sections from kinetics study over 4 weeks at a single treatment of 10 mg/kg. **(E)** Semiquantitative analysis of the extent of hybridization signal throughout the respiratory epithelium (described in detail in the Materials and Methods ''ISH analysis'' section). **(F)** A confocal microscope image of a mouse lung bronchus is presented following treatment with three doses of 10 mg/kg in WT mouse. The presented image is a stack of only DAPI-positive optical sections. *Blue*, nuclei (DAPI staining); *green*, Cy5-SPL84. ISH, *in situ* hybridization; IT, intratracheal.

images demonstrate the presence of SPL84 across the respiratory epithelium, including the epithelial cells in the bronchus and bronchioles, as well as in the distal alveoli regions (Supplementary Fig. S2A).

Further kinetics studies with SPL84 were performed up to 1 or 4 weeks post-dosing. The first study assessed kinetics over 1 week post-dose at two doses (5 or 10 mg/kg) (three treatments every other day), and sampling at four time points after last treatment (1, 3, 5, or 7 days). The results showed that SPL84 was distributed and retained in the lung at all time points, up to 7 days post-dosing. There was no prominent difference in hybridization pattern and signal strength between the different dose levels (5 mg/kg vs. 10 mg/kg) (Fig. 3B). SPL84 was detected in cells in all areas of the lung, including the trachea, bronchi, bronchioles, and alveoli (Supplementary Fig. S2B). A blinded semiquantitative evaluation of ISH signal in respiratory epithelium demonstrated that 3 days after the last administration, SPL84 was detected in >90% of epithelial surface cells, and 7 days after last administration, SPL84 was still widely spread along the epithelium (detected at 50–75% of the epithelial surface) (Fig. 3C).

The second kinetics study was performed for a longer period of 4 weeks after a single dose of 10 mg/kg and sampling at three time points (1, 2, or 4 weeks post-dose). The results showed that SPL84 was widely distributed and retained in the lungs for up to 4 weeks post-dosing, while vehicle control-treated animals showed no hybridization signal (Supplementary Fig. S4A). SPL84 was detected in respiratory epithelial cells at all parts of airways (Fig. 3D). A blinded semiquantitative evaluation of ISH signal in respiratory epithelium demonstrated that a high coverage of the epithelium surface with SPL84 was maintained from 1 week up to 4 weeks following a single SPL84 administration (Fig. 3E).

We additionally assessed the localization of SPL84 in mouse lung epithelial cell nuclei using a fluorescently labeled SPL84 following IT administration (three treatments every other day, 10 mg/kg). As can be seen in Fig. 3F, SPL84 penetrates epithelial cells along the bronchus and is localized within the cell nuclei and cytoplasm. Similar results were obtained in distal (alveoli) regions (Supplementary Fig. S3).

Altogether, the results in WT mouse lungs indicate that SPL84 is broadly distributed and is localized to the target region (nucleus) within the lung epithelial cells, in proximal as well as distal lung regions.

Broad pulmonary distribution of SPL84 in muco-obstructive mouse model

Following confirmation of wide SPL84 distribution in WT mice, we investigated whether SPL84 penetrates the mucus layer *in vivo* in a muco-obstructive mouse model, the β-ENaC mouse [30]. A comparable study was performed in WT and β-ENaC mice from identical background strains with SPL84, and the distribution of SPL84 was evaluated with ISH. No prominent differences in the hybridization patterns were found between the WT and β-ENaC mice lungs (Fig. 4A). Figure 4B presents the examples of the hybridization pattern in the airway compartments (main bronchi, bronchiole, and alveoli epithelial cells) of WT and β-ENaC mice, showing a similar hybridization signal located to the apical part of respiratory epithelial cells. A blinded semiquantitative evaluation of ISH signal demonstrated a high coverage of 90% in the lungs of both mouse types (WT and β-ENaC) (Fig. 4C). These results are aligned with previous studies that found that inhaled ASO penetrated through CF-like mucus in the β-ENaC mouse [31,32].

Broad lung distribution of inhaled SPL84 in monkey lungs

Monkeys are one of the large animal species frequently used for preclinical safety evaluation of drugs before clinical trials in humans. Monkeys bear close resemblance to humans

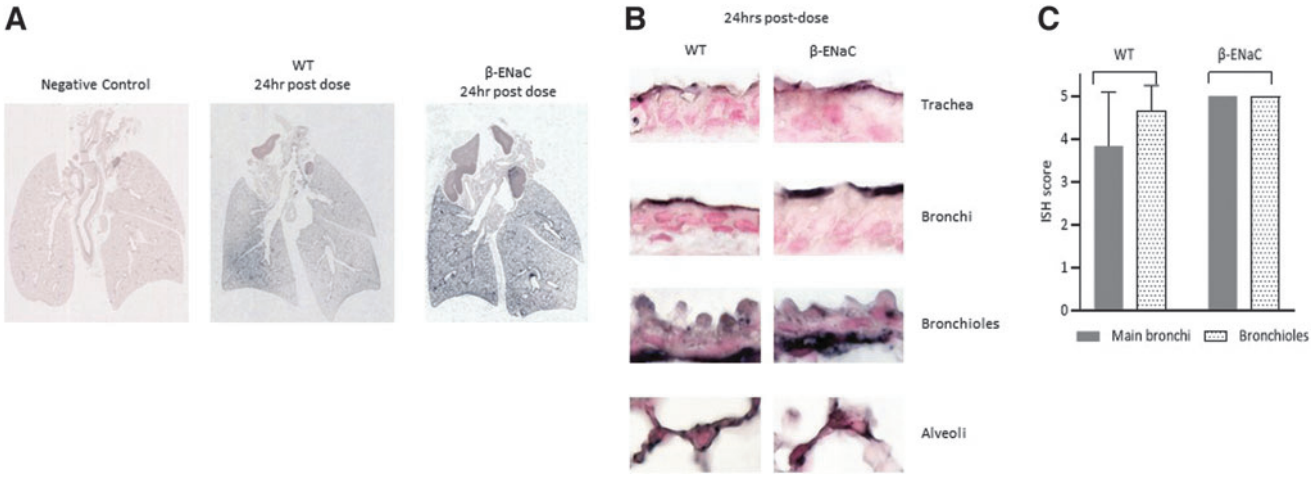

FIG. 4. SPL84 properly distributes through the mucus layer in a muco-obstructive mouse model, the β-ENaC mouse. **(A)** Low-resolution scans of sections from representative mice from different groups. From *left* to *right*: β-ENaC transgenic mice treated with saline, WT mice treated with 5 mg/kg of SPL84, β-ENaC mice treated with 5 mg/kg of SPL84. Additional control of WT mice treated with saline presented in Supplementary Fig. S4B. **(B)** High-power images of representative regions from WT (*left*) and β-ENaC (*right*) SPL84-treated mice at 5 mg/kg. **(C)** Semiquantitative analysis of the extent of hybridization signal throughout the respiratory epithelium (described in detail in the Materials and Methods ''ISH analysis'' section).

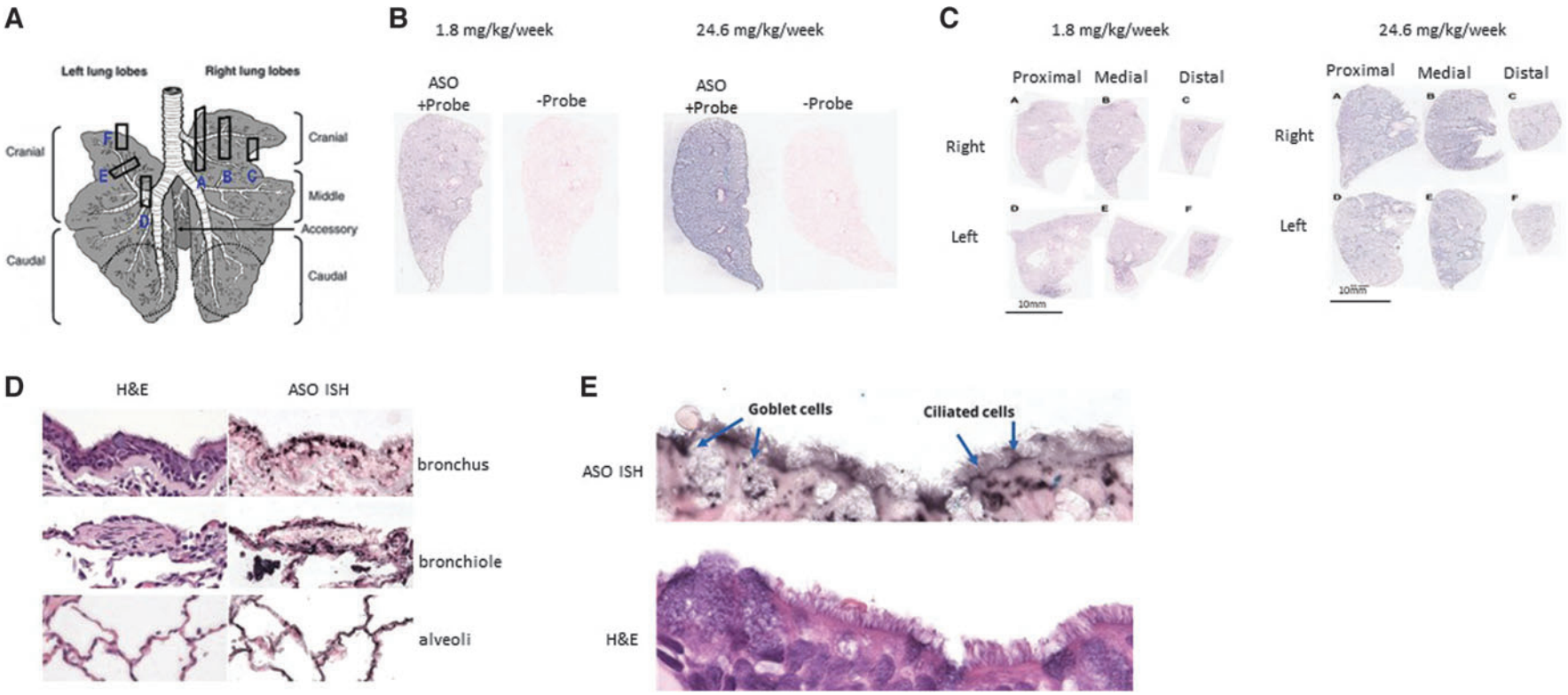

FIG. 5. Broad lung distribution of inhaled SPL84 in monkey lungs. **(A)** Schematic diagram of lung specimens collected for ISH study. **(B)** Representative images of a region of the monkey lung treated with low and high doses of SPL84 (1.8 or 24.6 mg/kg/week, respectively). **(C)** Low-power scans of monkey lung sections following inhaled treatment with 1.8 or 24.6 mg/kg/week SPL84 from all collected regions. **(D, E)** High-power (objective × 40) microphotographs of parallel H&E-stained and hybridized (ISH) sections of bronchial epithelium from 24.6 mg/kg/week treated monkeys. **(E)** Enlarged selected area of different types of epithelial cells is marked. H&E, hematoxylin–eosin.

in anatomical and physiological lung properties, providing a more adequate model system to study the lung distribution [33]. Therefore, it was important to evaluate ASO distribution in the monkey lungs.

SPL84 distribution was analyzed by ISH labeling of monkey lung sections following weekly inhalation of SPL84 for 4 weeks at low and high doses (1.8 and 24.6 mg/kg/week).

We observed broad SPL84 distribution throughout the lungs, which was dose dependent, and showed strong and uniform labeling in all sections sampled, from the proximal to the distal lung regions (Fig. 5A–C). SPL84 was detected across the respiratory epithelium (bronchi and bronchioles), as well as in the distal alveolar cells (Fig. 5D). A higher magnitude image also demonstrated that SPL84 enters different types of epithelial cells, including ciliated and secretory cells (Fig. 5E).

Discussion

Achieving optimal delivery and distribution of oligonucleotides to the lungs is in the scope of interest for many therapeutic approaches. We have developed SPL84, an inhaled ASO drug, targeted specifically for the treatment of CF patients carrying the 3849 mutation. The administration of SPL84 via inhalation allows local administration to the target organ, the lungs, with minimal systemic exposure [34]. One challenge of inhaled drug delivery for CF and other mucoobstructive diseases is the thick mucus layer covering the airways that can be an obstacle for drug delivery [20]. The comprehensive results presented in this study demonstrate that SPL84 is broadly distributed in WT and mucoobstructive mice and WT cynomolgus monkey lungs. These results are in agreement with previously published data [31,34,35]. Importantly, we demonstrated that inhaled SPL84 penetrates through the CF-like thick mucus layer into the epithelial cells both *in vitro* and *in vivo*. Moreover, since the lungs are made up of many different cell types, it was important to show that SPL84 enters different types of epithelial cells—ciliated as well as secretory (goblet) cells.

The proven durability of SPL84 for up to 4 weeks following a single dose in mice is supportive of a weekly/every other week inhalation regimen that will be further evaluated in clinical studies. This low frequency of administration will potentially provide a promising safety profile with reduced treatment burden on patients.

The demonstrated structural stability of the small size (estimated as 1 nm), single-strand, negatively charged SPL84 confirmed that additional vehicles or components to support SPL84 delivery to the lungs are not required [29]. On the contrary, it is proposed that larger, more complex inhaled RNA/DNA-based therapies such as mRNA replacement, DNA editing, or siRNA, which require delivery systems based on encapsulated LNPs/specific ligand conjugates to allow penetration to lung epithelial cells or other cells, might present some significant disadvantages. The physicochemical parameters of LNPs, including their size, shape, charge, and surface composition, directly impact cellular internalization efficiency and have also been associated with adverse immune events [36]. Finally, the larger size of these compounds results in significantly slower migration and penetration through even healthy mucus and will be further slowed under pathological conditions when the mesh size of mucus decreases.

Taken together, the combination of functional rescue by SPL84 demonstrated in patient-derived respiratory cells [14] with the proven efficient delivery to lung epithelial cells, along with the clinically validated chemical modifications (2′-O-MOE phosphorothioate [37,38]), generates a promising drug that could potentially provide a cure for the lung disease of CF in >1500 patients worldwide carrying the 3849 mutation. It is important to note that the inhaled ASO technology that was developed for SPL84 is the basis for additional ASO-based drugs that are currently being developed for additional CF mutations with unmet need as well as for other lung diseases. Using different ASO MoAs, a variety of mutation types can be targeted, including splicing, missense, and stop mutations. In addition, there are various other severe pulmonary diseases, such as bronchiectasis, asthma, chronic obstructive pulmonary disease, and idiopathic pulmonary fibrosis, which can benefit from our established inhaled platform delivery system and ASO technology.

Conclusions

Altogether, these data highlight the therapeutic potential and advantages of inhaled SPL84 for treating CF by effectively penetrating the pathological mucus barrier, allowing for targeted cellular uptake across the entirety of the lung. Successful production of functional WT CFTR protein for these patients will improve clinical outcomes in a population of people with CF that do not have efficient therapies and will potentially pave the way for a new generation of ASO-mediated therapies capable of treating various other severe pulmonary diseases.

Acknowledgments

The authors thank Tilley Stephen and Jania Corey (Division of Pulmonary Diseases and Critical Care Medicine, Department of Medicine, UNC) for the β-ENaC mice studies. β-ENaC mice were kindly provided by Wanda K. O'Neal (UNC). The authors also thank Alexander (Sasha) Faerman (Smart Assays) for the establishment of the methods and ISH analysis. The authors also thank Raanan Margalit [Science in Action (for executing all the mice studies)]. Microscopy images were acquired by Noemi Melamed (Bio Imaging Unit, Hebrew University).

Author Disclosure Statement

E.O.-G, L.F., O.B.-A., C.D.S., Y.S.O., B.K., and G.H. have been under the employment of SpliSense Ltd. M.R.M., W.B., K.R.R., and D.B.H. declare no competing interests.

Funding Information

This research was supported by SpliSense Ltd.

Supplementary Material

Supplementary Figure S1
Supplementary Figure S2
Supplementary Figure S3
Supplementary Figure S4
Supplementary Table S1

References

1. Sharma VK, RK Sharma and SK Singh. (2014). Antisense oligonucleotides: modifications and clinical trials. Med Chem Comm 5:1454–1471.
2. Bennett CF and EE Swayze. (2010). RNA targeting therapeutics: molecular mechanisms of antisense oligonucleotides as a therapeutic platform. Annu Rev Pharmacol Toxicol 50:259–293.
3. Kole R, AR Krainer and S Altman. (2012). RNA therapeutics: beyond RNA interference and antisense oligonucleotides. Nat Rev Drug Discov 11:125–140.
4. Groen EJN, K Talbot and TH Gillingwater. (2018). Advances in therapy for spinal muscular atrophy: promises and challenges. Nat Rev Neurol 14:214–224.
5. Dzierlega K and T Yokota. (2020). Optimization of antisense-mediated exon skipping for Duchenne muscular dystrophy. Gene Ther 27:407–416.
6. Hammond SM, A Aartsma-Rus, S Alves, SE Borgos, RAM Buijsen, RWJ Collin, G Covello, MA Denti, LR Desviat, et al. (2021). Delivery of oligonucleotide-based therapeutics: challenges and opportunities. EMBO Mol Med 13:1–23.
7. Orenti A, A Zolin, A Jung, J van Rens, A Fox, M Krasnyk, G Daneau, E Hatziagorou, M Mei-Zahav, et al. (2022). ECFSPR Annual Report 2020.
8. Cystic Fibrosis Foundation Patient Registry 2020 Annual Data Report Bethesda. https://www.cff.org/sites/default/files/2021-11/Patient-Registry-Annual-Data-Report.pdf.
9. KALYDECO® (ivacaftor) Tablets and Oral Granules. https://www.accessdata.fda.gov/drugsatfda_docs/label/2019/203188s029,207925s008lbl.pdf.2019.
10. SYMDEKO™ (tezacaftor/ivacaftor; ivacaftor) Tablets. https://www.accessdata.fda.gov/drugsatfda_docs/label/2018/210491lbl.pdf.2018.
11. TRIKAFTA®(elexacaftor/tezacaftor/ivacaftor;ivacaftor)Tablets. https://www.accessdata.fda.gov/drugsatfda_docs/label/2021/212273s008lbl.pdf.2021.
12. Kerem E, M Cohen-Cymberknoh, R Tsabari, M Wilschanski, J Reiter, D Shoseyov, A Gileles-Hillel, T Pugatsch, JC Davies, et al. (2021). Ivacaftor in people with cystic fibrosis and a 3849110kb C → T or D1152H residual function mutation. Ann Am Thorac Soc 18:433–441.
13. Anthony G, MD Durmowicz, A Badrul, MD Chowdhury and R Curtis. Symdeko tezacaftor-ivacaftor in combination. https://www.accessdata.fda.gov/drugsatfda_docs/nda/2018/210491Orig1s000SumR.pdf.2018.
14. Oren YS, M Irony-Tur Sinai, A Golec, O Barchad-Avitzur, V Mutyam, Y Li, J Hong, E Ozeri-Galai, A Hatton, C Leibson, et al. (2021). Antisense oligonucleotide-based drug development for cystic fibrosis patients carrying the 3849 + 10 kb C-to-T splicing mutation. J Cyst Fibros 20:865–875.
15. Clancy JP, CU Cotton, SH Donaldson, GM Solomon, DR VanDevanter, MP Boyle, M Gentzsch, JA Nick, B Illek, JC Wallenburg, et al. (2019). CFTR modulator theratyping: Current status, gaps and future directions. J Cyst Fibros 18:22–34.
16. McCarron A, D Parsons and M Donnelley. (2021). Animal and cell culture models for cystic fibrosis: which model is right for your application? Am J Pathol 191:228–242.
17. Pranke IM, A Hatton, J Simonin, JP Jais, F Le Pimpec-Barthes, A Carsin, P Bonnette, M Fayon,N Stremler-Le Bel, D Grenet, et al. (2017). Correction of CFTR function in nasal epithelial cells from cystic fibrosis patients predicts improvement of respiratory function by CFTR modulators. Sci Rep 7:7375.
18. Durmowicz AG, R Lim, H Rogers, CJ Rosebraugh and BA Chowdhury. (2018). The U.S. food and drug administration's experience with ivacaftor in cystic fibrosis: Establishing efficacy using in vitro data in lieu of a clinical trial. Ann Am Thorac Soc 15:1–2.
19. Mauroy B, P Flaud, D Pelca, C Fausser, J Merckx and BR Mitchell. (2015). Toward the modeling of mucus draining from human lung: role of airways deformation on air-mucus interaction. Front Physiol 6:1–15.
20. Hill DB, B Button M Rubinstein and RC Boucher. (2022).Physiology and pathophysiology of human airway mucus. Physiol Rev 102:1757–1836.
21. Hill DB, RF Long, WJ Kissner, E Atieh, IC Garbarine, MR Markovetz, NC Fontana, M Christy, M Habibpour, R Tarran, et al. (2018). Pathological mucus and impaired mucus clearance in cystic fibrosis patients result from increased concentration, not altered pH. Eur Respir J 52(6):1801297.
22. Rouillard KR, MR Markovetz, WJ Kissner, WL Boone, LM Plott and DB Hill. (2023). Altering the viscoelastic properties of mucus-grown Pseudomonas aeruginosa biofilms affects antibiotic susceptibility. Biofilm 5:100104.
23. Tenchov R, R Bird, AE Curtze and Q Zhou. (2021). Lipid nanoparticles from liposomes to mrna vaccine delivery, a landscape of research diversity and advancement. ACS Nano 15:16982–17015.
24. Conger BT, S Zhang, D Skinner, SB Hicks, EJ Sorscher, SM Rowe and BA Woodworth. (2013). Comparison of cystic fibrosis transmembrane conductance regulator (CFTR) and ciliary beat frequency activation by the CFTR modulators genistein, VRT-532, and UCCF-152 in primary sinonasal epithelial cultures. JAMA Otolaryngol Head Neck Surg 139:822–827.
25. Grubb B, J Harkema, W O'Neal, R Boucher and M Mall. (2004). Increased airway epithelial Na+ absorption produces cystic fibrosis-like lung disease in mice. Nat Med 10:487.
26. Goebl N, B Berridge, VJ Wroblewski and PL Brown-Augsburger. (2007). Development of a sensitive and specific in situ hybridization technique for the cellular localization of antisense oligodeoxynucleotide drugs in tissue sections. Toxicol Pathol 35(4):541–548.
27. Hill DB and B Button. (2012). Establishment of respiratory air-liquid interface cultures and their use in studying mucin production, secretion, and function. Methods Mol Biol 842:245–258.
28. Khvorova A and JK Watts. (2017). The chemical evolution of oligonucleotide therapies of clinical utility. Nat Biotechnol 35:238–248.
29. Juliano RL. (2018). Intracellular trafficking and endosomal release of oligonucleotides: what we know and what we don't. Nucleic Acid Ther 28:166–177.
30. Mall M, BR Grubb, JR Harkema, WKO Neal and RC Boucher. (2004). Increased airway epithelial Na + absorption produces cystic fibrosis-like lung disease in mice. Nat Med 10:487–493.
31. Crosby JR, C Zhao, C Jiang, D Bai, M Katz, S Greenlee, H Kawabe, M McCaleb, D Rotin, S Guo, et al. (2017). Inhaled ENaC antisense oligonucleotide ameliorates cystic fibrosis-like lung disease in mice. J Cyst Fibros 16:671–680.

32. Brinks V, K Lipinska, M Koppelaar, B Matthee, BM Button, A Livraghi-Butrico and N Henig. (2016). WS18.6 QR-010 penetrates the CF-like mucus barrier in vitro and in vivo. J Cyst Fibros 15:S31.
33. Guillon A, T Sécher, LA Dailey, L Vecellio, M de Monte, M Si-Tahar, P Diot, CP Page and N Heuzé-Vourc'h. (2018). Insights on animal models to investigate inhalation therapy: Relevance for biotherapeutics. Int J Pharm 536: 116–126.
34. Fey RA, MV Templin, JD McDonald, RZ Yu, JA Hutt, AP Gigliotti, SP Henry and MD Reed. (2014). Local and systemic tolerability of a 2′O-methoxyethyl antisense oligonucleotide targeting interleukin-4 receptor-α delivery by inhalation in mouse and monkey. Inhal Toxicol 26:452–463.
35. Karras JC, JR Crosby, M Guha, D Tung, DA Miller, WA Gaarde, RS Geary, BP Monia and SA Gregory. (2007). Anti-inflammatory activity of inhaled IL-4 receptor-α antisense oligonucleotide in mice. Am J Respir Cell Mol Biol 36:276–285.
36. Yang L, F Ma, F Liu, J Chen, X Zhao and Q Xu. (2020). Efficient delivery of antisense oligonucleotides using bioreducible lipid nanoparticles in vitro and in vivo. Mol Ther Nucleic Acids 19:1357–1367.
37. Mercuri E, BT Darras, CA Chiriboga, JW Day, C Campbell, AM Connolly, ST Iannaccone, J Kirschner, NL Kuntz, K Saito, et al. (2018). Nusinersen versus sham control in later-onset spinal muscular atrophy. N Engl J Med 378: 625–635.
38. Hua Y, K Sahashi, G Hung, F Rigo, MA Passini, CF Bennett and AR Krainer. (2010). Antisense correction of SMN2 splicing in the CNS rescues necrosis in a type III SMA mouse model. Genes Dev 24:1634–1644.

Address correspondence to:
Gili Hart, PhD
SpliSense, Biohouse Labs
Minrav Building
Haddasah Ein Kerem
Jerusalem
Israel

E-mail: gili@splisense.com

Received for publication March 19, 2023; accepted after revision July 25, 2023.